SUPPLEMENTARY INFORMATION for

IDENTIFICATION OF ESSENTIAL CANNABINOID-BINDING DOMAINS: STRUCTURAL INSIGHTS INTO EARLY DYNAMIC EVENTS IN RECEPTOR ACTIVATION

Joong-Youn Shim, Alexander C. Bertalovitz, and Debra A. Kendall

SUPPLEMENTARY EXPERIMENTAL PROCEDURES

Cross-correlation analysis—The MD analysis software g_correlation (1, 2) was used to create cross-correlation matrices from ~ 10,000 coordinates recorded every 2 ps from the last 20 ns of the MD simulations of **HU210-CB1y2** and **CP55940-CB1y**, respectively. Both the least squares fit and the non-linear generalized correlation were calculated using the Cα atoms of the receptor residues. To minimize any loss of the detail of interest from the full protein, the N-terminal end residues before H1 and the C-terminal end residues after H7 were not considered in this analysis.

Construction of the F174$^{2.61}$A and F177$^{2.64}$A mutant receptor models— The mutant receptor model was generated by replacing F174$^{2.61}$ or F177$^{2.64}$ in **HU210-CB1y3** at 35 ns of the simulation, at which time the receptor system appeared fully converged, with an Ala residue. After 1,500 steps of minimization, the mutant receptor system was simulated at 310 K for 21.7 ns in the NPT ensemble. The resulting mutant receptor models were compared with **HU210-CB1y3** at 53 ns.

SUPPLEMENTARY RESULTS AND DISCUSSION

Interactions of CP55940 in the minor binding pocket of the CB1 receptor—The region of the minor binding pocket under EC1 at the extracellular region by H2/H3/H7 appears to be important for the binding of CP55940 through H-bonding network around the salt bridge between D184^{EC1} and K192$^{3.28}$ (Supplementary Fig. 4). Thus, several coordinated water molecules and polar residues in this region are involved in H-bonding to the ligand: (i) The A-ring phenolic hydroxyl oxygen atom forms a water-mediated hydrogen bond to the side chain hydroxyl oxygen atom of S383$^{7.39}$. (ii) The A-ring phenolic hydroxyl oxygen atom of the ligand also forms another H-bond to a water molecule that forms a H-bond to the C-ring hydroxyl oxygen atom of the ligand; (iii) The C-ring hydroxyl oxygen atom of the ligand interacts with D184^{EC1}; and (iv) The C-ring propyl hydroxyl oxygen atom of the ligand interacts with C386$^{7.42}$ through H-bonding. Interestingly, the side chain hydroxyl oxygen atom of S173$^{2.60}$, one of the polar residues in this region, is not involved in ligand binding but loosely coordinated to a water molecule that in turn is coordinated by the side chain nitrogen atom of K192$^{3.28}$. Considering no alteration in CP55940 binding by the S173$^{2.60}$A mutation (3), the role of S173$^{2.60}$ is to partly stabilize the receptor. We observed that the A-ring hydroxyl of HU210 was close to the membrane surface and partly covered by solvent and EC2. In contrast, the A-ring hydroxyl group of CP55940 is stabilized by the water-mediated H-bonding to S383$^{7.39}$, suggesting an important role of S383$^{7.39}$ in CP55940 binding. In agreement, the S383$^{7.39}$A mutation is reportedly more detrimental to CP55940 than HU210 binding (3). Overall, it appears that the A/C-ring of CP55940 tightly binds to the polar/charged/aromatic residues in the region of the minor binding pocket.

SUPPLEMENTARY REFERENCES

1. http://www.mpibpc.mpg.de/home/grubmueller/downloads/GeneralizedCorrelations/index.html
2. Lange, O. F., and Grubmüller, H. (2006) *Proteins* **62**, 1053–1061
3. Kapur, A., Hurst, D. P., Fleischer, D., Whitnell, R., Thakur, G. A., Makriyannis, A., Reggio, P. H., and Abood, M. E. (2007) *Mol. Pharmacol*. **71**, 1512–1524

Supplementary Table 1. Molecular geometries of HU210 obtained by CHARMM in comparison with those obtained by ab initio RHF/6-31G* level calculations. The ligand structure was extracted from the last snapshot of **HU210-CB1y3** and subjected to a full optimization.

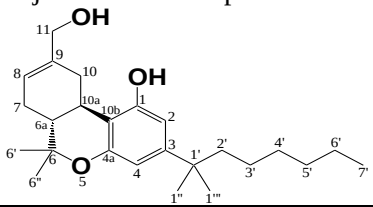

	RHF/6-31G*	CHARMM
r(C1-O)	1.354	1.385
r(C1-C2)	1.379	1.381
r(C1-C10b)	1.400	1.396
r(C2-C3)	1.399	1.412
r(C3-C4)	1.379	1.408
r(C3-C1')	1.538	1.536
r(C4-C4a)	1.396	1.379
r(C4a-O5)	1.349	1.352
r(C4a-C10b)	1.384	1.395
r(O5-C6)	1.428	1.415
r(C6-C6a)	1.535	1.548
r(C6-C6')	1.525	1.521
r(C6-C6'')	1.531	1.534
r(C6a-C10a)	1.539	1.536
r(C6a-C7)	1.531	1.551
r(C10a-C10b)	1.520	1.537
r(C10a-C10)	1.539	1.569
r(C7-C8)	1.507	1.505
r(C8=C9)	1.322	1.349
r(C9-C10)	1.513	1.511
r(C9-C11)	1.505	1.501
r(C11-O)	1.407	1.413
r(C1'-C2')	1.551	1.554
r(C1'-C1'')	1.537	1.551
r(C1'-C1''')	1.543	1.548
r(C2'-C3')	1.531	1.536
r(C3'-C4')	1.532	1.537
r(C4'-C5')	1.533	1.539
r(C5'-C6')	1.531	1.540
r(C6'-C7')	1.529	1.532
∠(O-C1-C2)	120.52	112.86
∠(O1-C1-C10b)	117.22	121.46
∠(C2-C1-C10b)	122.25	122.71
∠(C1-C2-C3)	121.03	121.39
∠(C2-C3-C4)	117.49	115.76
∠(C2-C3-C1')	119.71	120.39
∠(C4-C3-C1')	122.77	123.72
∠(C3-C4-C4a)	120.76	121.70
∠(C4-C4a-O5)	115.19	114.57

∠(C4-C4a-C10b)	122.60	122.59
∠(O5-C4a-C10b)	122.22	121.12
∠(C4a-O5-C6)	118.98	121.70
∠(O5-C6-C6a)	106.87	111.28
∠(O5-C6-C6’)	103.82	103.08
∠(O5-C6-C6’’)	108.87	109.24
∠(C6a-C6-C6’)	112.06	109.72
∠(C6a-C6-C6’’)	114.54	113.30
∠(C6’-C6-C6’’)	110.01	109.73
∠(C6-C6a-C10a)	112.43	109.84
∠(C6-C6a-C7)	115.65	113.91
∠(C10a-C6a-C7)	109.42	110.42
∠(C6a-C10a-C10b)	110.62	110.58
∠(C6a-C10a-C10)	107.72	107.67
∠(C10b-C10a-C10)	114.09	115.07
∠(C1-C10b-C4a)	115.70	115.60
∠(C1-C10b-C10a)	123.33	121.03
∠(C4a-C10b-C10a)	120.93	115.25
∠(C6a-C7-C8)	110.93	112.03
∠(C7-C8-C9)	123.91	124.16
∠(C8-C9-C10)	122.62	120.98
∠(C8-C9-C11)	121.09	122.00
∠(C10-C9-C11)	116.29	117.02
∠(C10a-C10-C9)	111.87	114.62
∠(C9-C11-O)	109.41	107.29
∠(C3-C1’-C2’)	110.66	109.87
∠(C3-C1’-C1’’)	112.27	112.73
∠(C3-C1’-C1’’’)	108.85	108.16
∠(C2’-C1’-C1’’)	109.50	110.34
∠(C2’-C1’-C1’’’)	108.18	109.61
∠(C1’’-C1’-C1’’’)	107.24	106.01
∠(C1’-C2’-C3’)	116.62	114.83
∠(C2’-C3’-C4’)	111.86	112.67
∠(C3’-C4’-C5’)	114.70	114.00
∠(C4’-C5’-C6’)	114.86	114.46
∠(C5’-C6’-C7’)	112.61	114.15
∠(O-C1-C2-C3)	-177.83	164.30
∠(C10b- C1-C2-C3)	1.41	3.60
∠(O-C1-C10b-4a)	174.95	-163.88
∠(O-C1-C10b-10a)	-3.02	-47.84
∠(C2-C1-C10b-C4a)	-4.32	-4.80
∠(C2-C1-C10b-C10a)	177.72	-153.07
∠(C1-C2-C3-C4)	1.46	-2.36
∠(C1-C2-C3-C1’)	179.78	-178.45
∠(C2-C3-C4-C4a)	-1.23	2.79
∠(C1’-C3-C4-C4a)	-179.49	178.74
∠(C2-C3-C1’-C2’)	57.62	61.69

∠(C2-C3-C1'-C1'')	-179.71	-174.80
∠(C2-C3-C1'-C1''')	-61.14	-57.92
∠(C4-C3-C1'-C2')	-124.16	-114.08
∠(C4-C3-C1'-C1'')	-1.49	9.43
∠(C4-C3-C1'-C1''')	117.09	126.31
∠(C3-C4-C4a-O5)	178.14	-169.67
∠(C3-C4-C4a-C10b)	-1.92	-4.47
∠(C4-C4a-O5-C6)	-158.18	-144.27
∠(C10b-C4a-O5-C6)	21.88	50.29
∠(C4-C4a-C10b-C1)	4.6	5.22
∠(C4-C4a-C10b-C10a)	-177.41	155.55
∠(O5-C4a-C10b-C1)	-175.50	169.47
∠(O5-C4a-C10b-C10a)	2.52	-40.20
∠(C4a-O5-C6-C6a)	-51.61	-56.76
∠(C4a-O5-C6-C6')	-170.22	-174.29
∠(C4a-O5-C6-C6'')	72.62	69.08
∠(O5-C6-C6a-C10a)	59.51	56.13
∠(O5-C6-C6a-C7)	-173.82	-179.42
∠(C6'-C6-C6a-C10a)	172.61	169.56
∠(C6'-C6-C6a-C7)	-60.72	-65.99
∠(C6''-C6-C6a-C10a)	-61.16	-67.43
∠(C6''-C6-C6a-C7)	65.51	57.03
∠(C6-C6a-C10a-C10b)	-38.22	-44.96
∠(C6-C6a-C10a-C10)	-163.54	-171.45
∠(C7-C6a-C10a-C10b)	-168.17	-171.41
∠(C7-C6a-C10a-C10)	66.52	62.10
∠(C6-C6a-C7-C8)	-176.66	-172.54
∠(C10a-C6a-C7-C8)	-48.48	-48.39
∠(C6a-C10a-C10b-C1)	-174.83	-174.57
∠(C6a-C10a-C10b-C4a)	7.30	37.05
∠(C10-C10a-C10b-C1)	-53.20	-52.33
∠(C10-C10a-C10b-C4a)	128.94	159.30
∠(C6a-C10a-C10-C9)	-48.47	-46.12
∠(C10b-C10a-C10-C9)	-171.69	-169.92
∠(C6a-C7-C8-C9)	14.08	17.53
∠(C7-C8-C9-C10)	3.12	-1.58
∠(C7-C8-C9-C11)	-176.15	178.95
∠(C8-C9-C10-C10a)	15.04	16.54
∠(C11-C9-C10-C10a)	-165.65	-163.96
∠(C8-C9-C11-O)	-120.52	-108.03
∠(C10-C9-C11-O)	60.16	72.47
∠(C3-C1'-C2'-C3')	60.94	58.84
∠(C1''-C1'-C2'-C3')	-63.34	-66.06
∠(C1'''-C1'-C2'-C3')	-179.90	177.57
∠(C2'-C3'-C4'-C5')	-175.09	-177.78
∠(C3'-C4'-C5'-C6')	-66.03	-67.30
∠(C4'-C5'-C6'-C7')	-176.09	-176.75

SUPPLEMENTARY FIGURE LEGENDS

Supplementary Figure 1. Some key torsional energy barriers of HU210 (**A**), Δ^9-THC (**B**), and CP55940 (**C**), obtained by CHARMM in comparison with those obtained by ab initio MP2/6-31G* level calculations. For HU210 and Δ^9-THC, the torsion angles with respect to (i) the bond connecting the A-ring and the C3 alkyl chain and (ii) the bond connecting the first and second carbons of the C3 alkyl chain were selected. For CP55940, the torsion angle with respect to the bond connecting the A-ring and the C-ring was selected.

Supplementary Figure 2. Comparison of the W356$^{6.48}$ rotamer changes in **HU210-CB1y2** (**A**) and in **CP55940-CB1y** (**B**). i. The rotameric angles, the χ1 angles (in black) and the χ2 angles (in red), of F170$^{2.57}$. ii. Superposition of the initial structure (in orange) and the final structure (in silver) of the simulation with respect to the backbone atoms of TMHs except H5 and H6. Only the TM helices are represented in ribbon. The side chains of C355$^{6.47}$ residues (in atom type: C, cyan; O, red; and H, white) of these structures are also presented by stick. Hydrogen atoms are omitted for clarity. iii. Cross correlation of **HU210-CB1y2** and **CP55940-CB1y**. X- and y-axes are the receptor H1 through H7; red indicates highly correlated movement (1.0) and blue indicates less correlated (0.0). Coupling between H5 and H6 are indicated by dotted lines (in black).

Supplementary Figure 3. **A.** The RMSDs (i) of the F174$^{2.61}$A mutant receptor (in black) and F177$^{2.64}$A mutant receptor (in orange), calculated by RMS fitting to the initial coordinates with respect to the backbone heavy atoms of the TM helical residues of the receptor. Superposition of the F174$^{2.61}$A (in grey) and F177$^{2.64}$A (in brown) mutant receptors to the wild-type (**HU210-CB1y3**) (in green), with respect to the backbone atoms of TMHs, viewed from the extracellular side (ii) and the membrane side (iii). The movement of H2 toward the TM central region in the F174$^{2.61}$A and F177$^{2.64}$A mutant receptors, along with the movement of the ligand, is represented by arrows. HU210 in the wild-type is colored in blue, HU210 in the F174$^{2.61}$A mutant is colored in grey, and HU210 in the F177$^{2.64}$A mutant is colored in brown. H1, H4, and H5 are omitted for clarity. **B.** i. The aromatic ring centroid distance between the A-ring of HU210 and F177$^{2.64}$ (in red) in the F174$^{2.61}$A mutant receptor or F174$^{2.61}$ (in black) in the F177$^{2.64}$A mutant receptor. ii. The aromatic ring centroid distances between F177$^{2.64}$ and the neighboring aromatic residues in the F174$^{2.61}$A mutant receptor. Color coding: F177$^{2.64}$/H178$^{2.65}$, blue; F177$^{2.64}$/H181$^{2.68}$, orange; and F177$^{2.64}$/F379$^{7.35}$, magenta. iii. The aromatic ring centroid distances between F174$^{2.61}$ and the neighboring aromatic residues in the F177$^{2.64}$A mutant receptor. Color coding: F174$^{2.61}$/F170$^{2.57}$, black; and F174$^{2.61}$/H178$^{2.65}$, green.

Supplementary Figure 4. Estimated nonbonding interaction energies of the A-ring of (i) HU210, (ii) Δ^9-THC, or (iii) CP55940 with: F189$^{3.25}$ (in black), F379$^{7.35}$ (in red), and F189$^{3.25}$/F379$^{7.35}$ (in green). Only the side chains of residues were considered in calculating the non-bonding energies. The energy values (in kcal/mol), with the standard deviation in parenthesis, averaged over the last 20.0 ns of the simulation are: -1.23(0.49), -2.15(0.99), and -3.38(1.17) for HU210; -0.79(0.31), -0.86(0.70), and -1.65(0.74) for Δ^9-THC; and -0.66(0.30), -1.31(0.84), and -1.97(0.72) for CP55940.

Supplementary Figure 5. Interactions of CP55940 in the minor binding pocket of the CB1 receptor in **CP55940-CB1y** at the end of the simulation. The ligand is represented by space-filling, the amino acids by stick, and the water molecules by ball-and-stick. The ligand is colored by atom type. The aromatic residues F177$^{2.64}$, F189$^{3.25}$, F268^{EC2}, and F379$^{7.35}$ are colored green. The salt bridge-forming D184^{EC1} and K192$^{3.28}$ are colored by atom type. H-bonds are represented by pink dotted lines. Hydrogen atoms of the amino acids are omitted for clarity. H1 and H2 are omitted for clarity. Color coding: C, cyan; O, red; N, blue; and H, white.

Supplementary Fig. 1

A

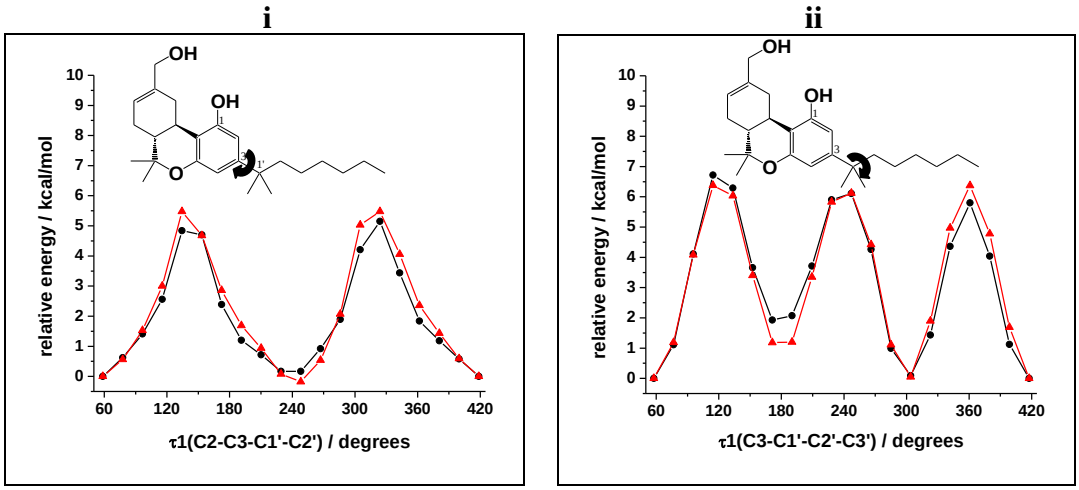

B

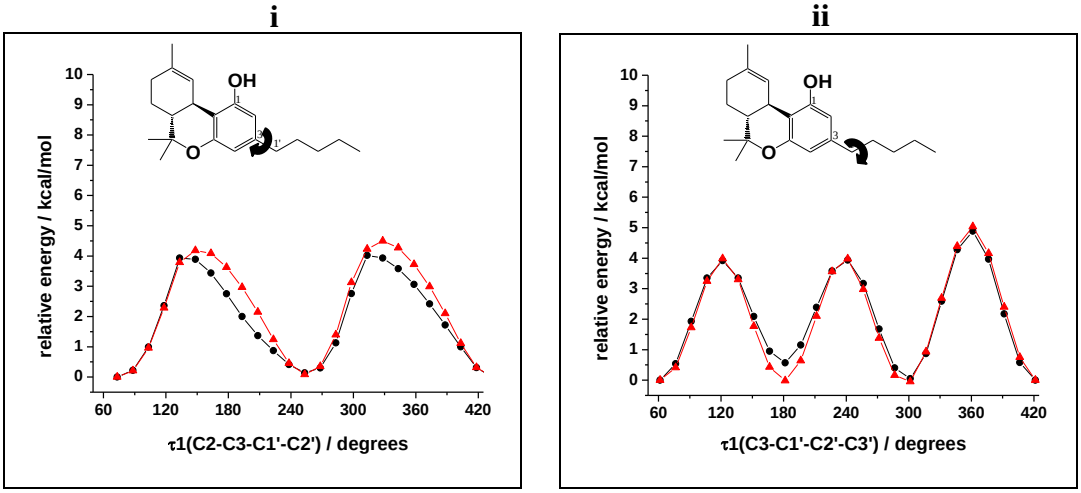

C

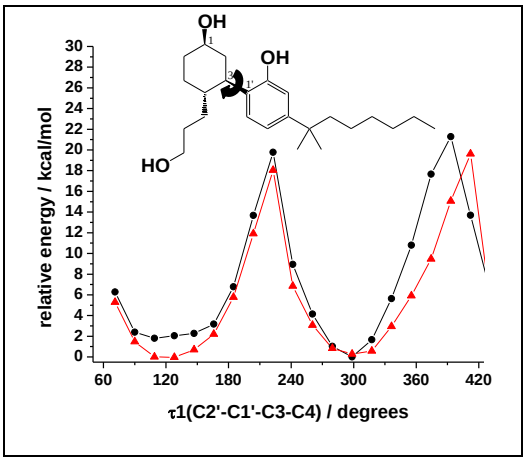

Supplementary Fig. 2

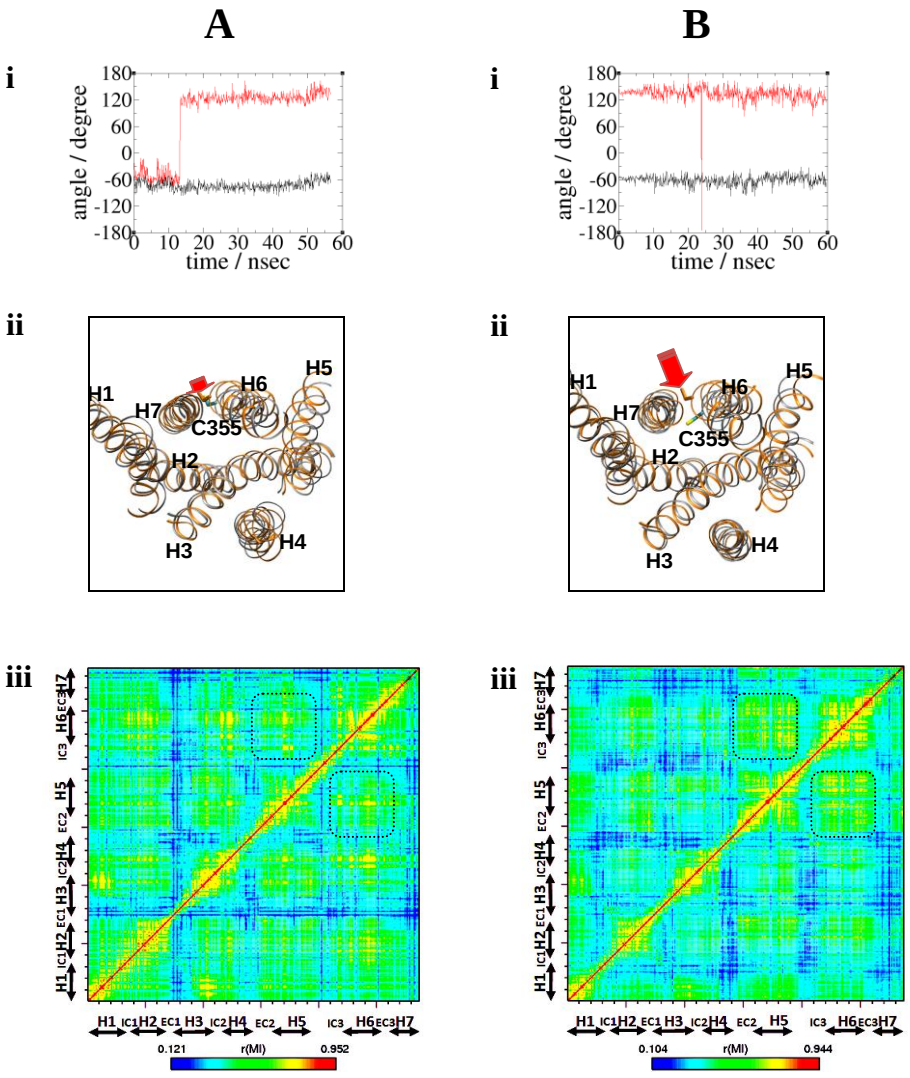

Supplementary Fig. 3

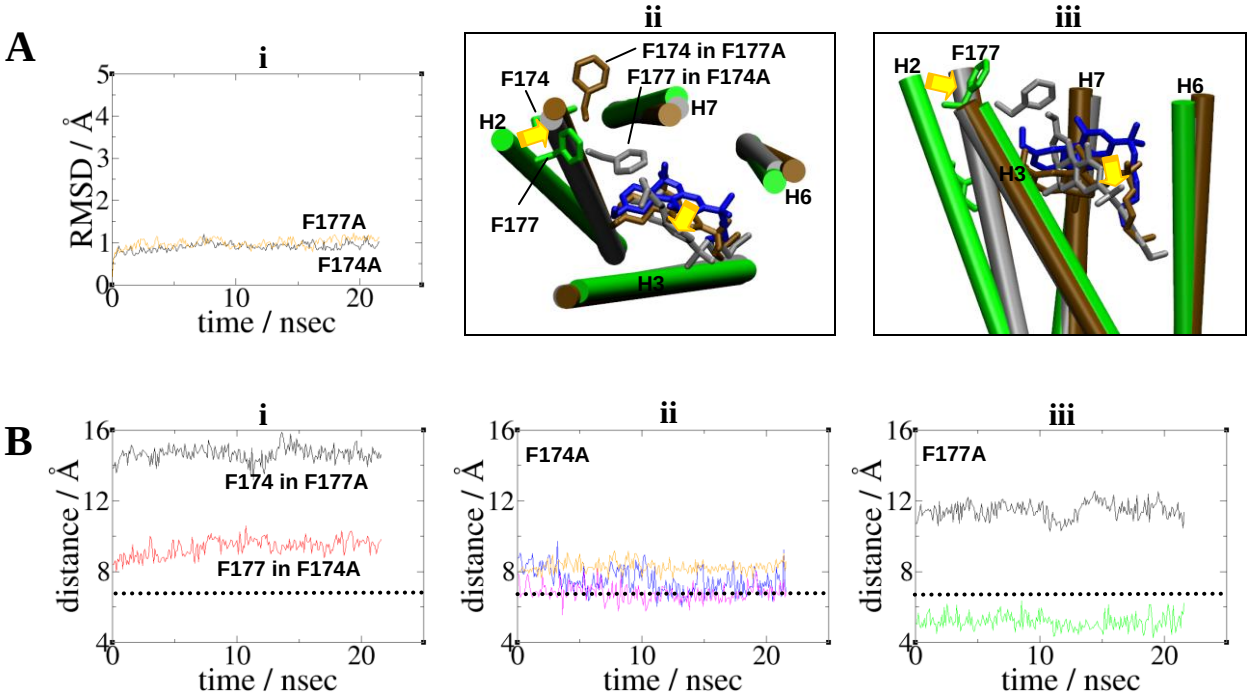

Supplementary Fig. 4

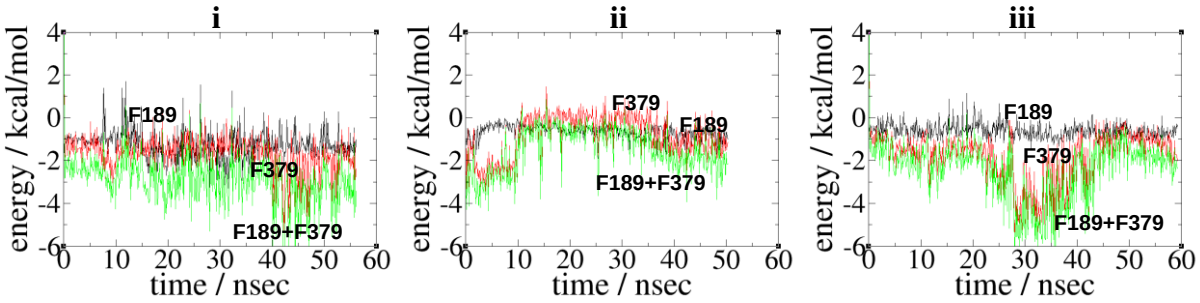

Supplementary Fig. 5